Deep pionic bound states in a nonlocal optical potential

Dinghui H. Lu and Rubin H. Landau
Physics Department, Oregon State University, Corvallis, Oregon 97331
(Received 6 August 1993; revised manuscript received 26 October 1993)

Pion-nucleus bound states are investigated in momentum space using a microscopic optical potential with energy dependences and nonlocalities arising from elementary potential models. We confirm the existence of deep, hybrid Coulomb-nuclear $1s$, $2s$, and $2p$ bound states, but find them to be considerably broader ($\sim$ 20–300 %) than reported previously for other potentials and slightly ($\sim$ 7%) more bound. Although the states still remain nonoverlapping, their larger widths may affect experimental searches.

PACS number(s): 36.10.Gv, 03.65.Ge

I. INTRODUCTION

When an optical potential is used as a model of a pionic atom, the imaginary part of the potential simulates the nuclear absorption of the pion. If the absorption is very strong, the effect of the potential is nonperturbative in that an *increase* in the imaginary part may lead to a *decrease* in the imaginary part of the binding energy (the level width) [1]. In this case, the increase in the imaginary potential reduces the wave function in the nuclear interior which reduces the wave function's overlap with the nucleus, and consequently reduces the level's width. Thus an optical potential with a large imaginary part is "repulsive" since it excludes the wave function from the nucleus and may lead to narrow states.

Recently, theoretical studies by Friedman and Scoff [2], Hirenzaki *et al.* [3], and Toki and Yamazaki [4,5] have pointed out that the optical potential for deeply bound levels of pions in heavy nuclei is sufficiently absorptive for there to exist narrow states. While these states are "quasibound" because they decay, they are also "quasistable" (and thus observable) because their widths are smaller than the energy-level spacings. For example, ^{208}Pb has the $(1s, 2p)$ states bound by $\sim (7, 5)$ MeV with widths $\simeq$ 0.5 MeV — in contrast to the $\sim$ 20 MeV widths expected if lowest-order perturbation theory were valid. In contrast to nuclear bound states in which the pion resides within the nucleus, these deep states are hybrid Coulomb-nuclear ones in which the pion's probability density peaks just outside the nuclear surface.

Observing deeply bound pion states in heavy nuclei is difficult because the x ray cascade ends with the pion being absorbed before it reaches the deep levels. Because transitions to the $1s$ level are seen experimentally only for $Z < 12$ and to the $2p$ level only for $Z < 30$, alternative observational methods have been proposed. A recent experimental search using the (n, p) transfer reaction did not record the distinct peaks expected for a $1s$ or $2p$ transition in Pb [6], which indicated that the cross sections are smaller, the widths larger, or the binding energies less certain than predicted. Other suggested experiments include (n, d) pickup [7], (π^-, γ) radiative trapping [8], and (π^-, p) pickup [9].

Most calculations of pion bound states use the phenomenological Ericson-Ericson potential:

$$V^{\rm opt}(r) \simeq \frac{-4\pi}{2\mu}[b_0\rho(r) + c_0\nabla\cdot\rho(r)\nabla + B_0\rho^2(r) + C_0\nabla\cdot\rho^2(r)\nabla] \quad (1)$$

with the parameters (b_0, c_0, B_0, C_0) determined by global fits to pionic atom energy levels. (For clarity we assume an isoscalar nucleus and leave off the Lorenz-Lorentz factor.) The key assumption behind (1) is that the πN and πNN interactions are of zero range and that πNT matrix is

$$\langle \mathbf{k}', \mathbf{p}'|t|\mathbf{k}, \mathbf{p}\rangle \propto b_0 + c_0\mathbf{k}'\cdot\mathbf{k} \quad (2)$$

for off-shell values of the pion and nucleon momenta and energies [10,11]. In contrast, we have investigated deeply bound states pion supported by a theoretical optical potential used previously only for pion scattering [10–12]. This potential has nonlocalities, unitarity off-shell behaviors, energy and momentum dependencies arising from separable pi-nucleon potentials, and a careful treatment of relativistic kinematics. The πN amplitudes are derived from πN scattering data and used for the analytic continuation to subthreshold complex energies. In contrast, the phenomenological potential (1) fits (b_0, c_0) to atomic data and then assumes they are constant, even though the predicted states are bound by $\sim$ 10 MeV. Considering the difficulty of experimentally observing deeply bound pion states, we aim in this paper to confirm their existence and provide alternate predictions of their energies and widths.

We work in momentum space and identify bound-state energies with the complex energy poles of the T matrix for the combined Coulomb plus nuclear potentials. This analytically continues the energy dependence of the optical potential to the complex bound-state energy — a procedure for which there is no coordinate space equivalent. Inversely, there is no precise, direct-momentum space treatment of the Ericson-Ericson potential (1) due to its singularity as $k = k' \to \infty$ [10,11]. Furthermore, it is not possible for us to simply remove the nonlocal-

ities in our calculation in order to make a comparison with the potential (1)—they are inherent in the potential. We have, however, in the previous pion-nucleus *scattering* calculations [10–12] demonstrated the significant sensitivities to off-shell and few-body effects, and since the bound-state shifts and widths are essentially proportional to the pion-nucleus scattering lengths and volumes, we expect similar sensitivities for bound states.

In Sec. II A we describe the optical and electromagnetic potentials; in Sec. II B we describe the computational method, and in Appendix A we establish the numerical precision of the computation and examine the importance of the relativistic wave equation. In Sec. III A we make comparisons to the experimental energies and widths of shallow states, and in Sec. III B we examine the deep states supported by our potential.

II. THEORY

A. The optical potential

The pion-nucleus interaction is described by the sum of electromagnetic plus optical potentials:

$$\langle \mathbf{k}'|V_E|\mathbf{k}\rangle = V^{\rm Coul}(q) + V^{VP}(q) + U_E^{(1)}(\mathbf{k}',\mathbf{k}) + U_E^{(2)}(\mathbf{k}',\mathbf{k}), \tag{3}$$

TABLE I. Parameters used in modified Wood-Saxon densities (R and a in fm).

	R_p	a_p	w_p	R_n	a_n	w_n
^{16}O	2.608	0.513	-0.051	2.608	0.461	-0.051
^{18}O	2.634	0.513	0.0	2.72	0.447	0.0
^{40}Ca	3.669	0.584	-0.102	3.669	0.584	-0.102
^{44}Ca	3.70	0.55	0.0	3.82	0.505	0.0
^{108}Ag	5.32	0.52	0.0	5.47	0.473	0.0
^{208}Pb	6.624	0.549	0.0	6.624	0.549	0.0
^{209}Bi	6.609	0.545	0.0	6.88	0.5	0.0

$$V^{\rm Coul}(q) = -\frac{Z\alpha\rho_p(q)}{2\pi^2 q^2}\ , \tag{4}$$

$$V^{VP}(q) = -\frac{Z\alpha^2\rho_p(q)}{2\pi^3}\int_1^\infty \frac{(2t^2+1)(t^2-1)^{1/2}}{3t^4[q^2+(2t/\lambda_e)^2]}dt. \tag{5}$$

Here the momentum transfer $\mathbf{q} = \mathbf{k}' - \mathbf{k}$, the Coulomb potential $V^{\rm Coul}$ is for a nucleus of finite size, the proton form factor is $\rho_p(q)$, the order-$Z\alpha^2$ vacuum polarization (Uehling) potential [13,14] is V^{VP}, and the electron Compton wavelength is λ_e. The first order optical potential is evaluated in the impulse and factored approximations:

$$U_E^{(1)}(\mathbf{k}',\mathbf{k}) = Z\langle \mathbf{k}', \mathbf{p}_0 - \mathbf{q}\,|t^{\pi p}_{\omega_{3B}}|\,\mathbf{k}, \mathbf{p}_0\rangle\,\rho_p(q) + N\langle \mathbf{k}', \mathbf{p}_0 - \mathbf{q}\,|t^{\pi p}_{\omega_{3B}}|\,\mathbf{k}, \mathbf{p}_0\rangle\,\rho_n(q)\ , \tag{6}$$

$$\langle \mathbf{k}', \mathbf{p}_0'\,|t|\,\mathbf{k}, \mathbf{p}_0\rangle = \frac{\gamma}{2\pi^2}\sum_\alpha \frac{g_\alpha(\kappa')g_\alpha(\kappa)}{D_\alpha(\omega_{3B})}P_l(\cos\theta_{\kappa'\kappa}), \tag{7}$$

$$D_\alpha(\omega) = \frac{1}{\sigma_\alpha} - \frac{2}{\pi}\int_{\xi P - P_F}^{\xi P + P_F} \frac{g_\alpha^2(\kappa)Q_0(P,\kappa)}{\omega - E_\pi(\kappa) - E_N(\kappa) + i\epsilon}\kappa^2 d\kappa. \tag{8}$$

Here $\alpha = ilj$ labels the πN eigenchannel ($i = \pi N$ isospin, l = orbital, and j = total angular momentum), σ_α is the sign of the potential, and κ and κ' are the initial and final πN COM momenta. We take the nuclear form factors $\rho_{p,n}(q)$ as Fourier transforms of Woods-Saxon densities [10] with the size parameters given in Table I (these are the standard set used by Friedman *et al.* [15] with an extension to Pb [16]). The Fredholm determinant (8) is modified to include Pauli blocking by using an angle-averaged Pauli operator Q_0. Since our model has finite range πN interactions, inclusion of a Lorentz-Lorenz term is inappropriate [12,17].

The two-body T matrices and momenta in (6) are related to off-shell ones in the πN COM by a Lorentz covariant prescription which determines γ, κ, and κ'. We include nucleon recoil by making the "optimal" choice for the momentum of the struck nucleon,

$$\mathbf{p}_0 = -\frac{\mathbf{k}}{A} + \frac{(A-1)\mathbf{q}}{2A}, \tag{9}$$

which is optimal in producing the best factored approximation and the most consistent off-energy-shell kinematics. We include additional recoil and Fermi motion effects by use of a three-body model in which a pion of momentum $\mathbf{k}$ scatters from a nucleon of momentum $\mathbf{p}_0$ outside of a passive core of momentum $\mathbf{P} = -(\mathbf{k}+\mathbf{p}+\mathbf{p}_0)$. This leads [12] to a πN subenergy for (6) of the form:

$$\omega_{3B}^2(E) = (k_\pi^\mu + k_A^\mu - P^\mu)^2 \simeq [E + m_\pi + m_A - E_{A-1}(P) - E_B]^2 - P^2, \tag{10}$$

where E_B is an effective core-nucleon binding energy we keep fixed at 20 MeV.

The second-order potential

$$U_E^{(2)}(\mathbf{k}',\mathbf{k}) = -\frac{4\pi A^2}{2\mu_{\pi A}(2\pi)^3}\left[B_0(E)\frac{\hat g_s(\kappa)\hat g_s(\kappa')}{\hat g_s^2(\kappa_0)} + C_0(E)\frac{\hat g_p(\kappa)\hat g_p(\kappa')}{\hat g_p^2(\kappa_0)}\boldsymbol{\kappa}'\cdot\boldsymbol{\kappa}\right]\rho^2(q), \tag{11}$$

$$\hat g_s(\kappa) = \frac{1}{\alpha_s^2+\kappa^2},\quad \hat g_p(\kappa) = \frac{1}{(\alpha_p^2+\kappa^2)^2} \tag{12}$$

includes, phenomenologically, contributions from all higher-order processes in ρ such as virtual nuclear excitation and pion annihilation. It is important for pionic atoms, since its imaginary part produces the levels' widths (the imaginary part of $U^{(1)}$ vanishes along the subthreshold real-energy axis). This form is a generalization of the separable form used for $U^{(1)}$, corresponding to a finite-ranged force (we take $\kappa_0 \to 0$ for subthreshold extrapolation). Unfortunately, it was impossible for us to reliably determine $U^{(2)}$ microscopically, or to analytically continue the energy dependence of phenomenological B_0 and C_0 to subthreshold energies.

B. Computational method

We solve the relativistic Schrödinger equation [18]

$$K(k)\psi_l(k) + \frac{2}{\pi}\int_0^\infty V_l(k,k';E)\psi_l(k')k'^2dk' = E\psi_l(k), \tag{13}$$

where $K(k) = \sqrt{m_\pi^2+k^2} + \sqrt{m_A^2+k^2} - m_\pi - m_A$ is the relativistic kinetic energy, and $V_l(k,k';E)$ is the energy-dependent pion-nucleus potential after partial wave projection. To incorporate the appropriate boundary conditions—even for the general case of coupled and open channels—we transform (13) to an integral equation involving the Green's function [19]:

$$|\psi\rangle = G_E V_E|\psi\rangle, \tag{14}$$

$$\psi_l(k) = \frac{2}{\pi}\frac{1}{E-K(k)}\int_0^\infty V_l(k,k';E)\,\psi_l(k')k'^2dk', \tag{15}$$

where for bound states there is no incident wave $|\phi\rangle$ in (14) and no $+i\epsilon$ in G_E. If we consider V_E, K, and G_E as operators or their matrix representation, we see that a solution of the eigenvalue problem (13) is equivalent to demanding nontrivial solutions of (14), namely,

$$(1 - G_E V_E)\,|\psi\rangle = 0 \quad \Rightarrow \quad \det|1 - G_E V_E| = 0. \tag{16}$$

Solving (16) is equivalent to determining the energies of the poles of the π-nucleus T matrix.

We search for solutions of (16) in complex energy space after removing the Coulomb singularity with the Landé subtraction technique. In contrast, the momentum space formulations of Kwon and Tabakin [13] and Cieplý *et al.* [20] directly solve (13) as an eigenvalue problem (Kwon and Tabakin use the Landé subtraction, and Cieplý *et al.* use the Vincent-Phatak cutoff). In further contrast, Kalbermann *et al.* [17] have solved a Coulomb plus nonlocal nuclear potential problem as an integrodifferential wave equation in coordinate space (a technique which would not include the full energy dependence of a separable πN T matrix).

Once the eigenenergies are known, we solve for the momentum space wave functions by using inverse iteration [13] on the Schrödinger equation (13):

$$[\psi_l(k_i)] = [H_E - E]^{-1}\,[\psi_l(k_i)]\,. \tag{17}$$

TABLE II. Effect of different treatments of relativity on point-Coulomb binding energies for $\pi^-{}^{40}$Ca atom. Compared are the analytic Schrödinger equation, the numeric Schrödinger equation, the relativistic Schrödinger equation, the Klein-Gordon equation with reduced mass, and the Klein-Gordon equation with pion mass. All energies in keV.

nl	$E_{\rm SE}$(anal)	$E_{\rm SE}$(num)	$E_{\rm RSE}$	$E_{\rm KGE}(\mu)$	$E_{\rm KGE}(m_\pi)$
$1s$	-1.4809	-1.4810	-1.5161	-1.5234	-1.5287
$2s$	-0.3702	-0.37025	-0.3761	-0.3772	-0.3785
$2p$	-0.3702	-0.37024	-0.3714	-0.3717	-0.3730

The normalization constraint $1 = \int_0^\infty \psi_l^2(k)\,k^2dk$ implies

$$1 = \int_0^\infty \left[\mathrm{Re}^2\psi_l(k) - \mathrm{Im}^2\psi_l(k)\right]\,k^2dk, \tag{18}$$

$$0 = \int_0^\infty \mathrm{Re}\;\psi_l(k)\,\mathrm{Im}\;\psi_l(k)\,k^2dk. \tag{19}$$

This normalization condition on the square of the complex wave function — as opposed to the modulus squared — follows from the Gamow-state formalism of Hernàndez and Mondragon [21]. By requiring the overlap of Re $\psi_l(k)$ and Im $\psi_l(k)$ to vanish, it often introduces an oscillation in Re $\psi_l(r)$. The coordinate space wave function is obtained via the Bessel transform:

$$\psi_l(r) \equiv \frac{u_l(r)}{r} = i^l\left(\frac{2}{\pi}\right)^{1/2}\int_0^\infty \psi_l(k)\,j_l(kr)\,k^2dk. \tag{20}$$

III. RESULTS

As indicated in Tables II and III of Appendix A, the predictions of pion-point Coulomb bound-state energies from the relativistic Schrödinger equation and the Klein-Gordon equation using a reduced mass differ by less than 1%. While we also found that ignoring $(V^{\rm opt})^2$ term in the Klein-Gordon equation may have a several percent effect (consistent with that found for $K^-{}^{32}$S [13]), in a practical sense this may not be important once the parameters of the $U^{(2)}$ are fit to data.

TABLE III. Effect of different treatments of relativity on point-Coulomb binding energies (in MeV) for $\pi^-{}^{208}$Pb atom via Schrödinger equation, relativistic Schrödinger equation (numeric), and Klein-Gordon equation (which has no s states for $Z\alpha > \frac{1}{2}$).

nl	$E_{\rm SE}$	$E_{\rm RSE}$	$E_{\rm KGE}$
$1s$	-24.97	-42.53	n
$2s$	-6.243	-9.224	n
$2p$	-6.242	-6.584	-6.607
$3s$	-2.775	-3.659	n
$3p$	-2.775	-2.921	-2.929
$3d$	-2.774	-2.824	-2.829
$4s$	-1.562	-1.930	n
$4p$	-1.561	-1.632	-1.636
$4d$	-1.562	-1.592	-1.593
$4f$	-1.560	-1.574	-1.577

TABLE IV. Theoretical and experimental shifts and widths in keV.

State	Ref.	ReE	$\epsilon_{\rm lpott}$	$\epsilon_{\rm exp}$	$\Gamma_{\rm lpott}$	$\Gamma_{\rm exp}$
$1s\,^{16}$O	[22]	-219.98	-14.57	-15.4 ± 0.1	8.14	7.92 ± 0.32
$2p\,^{16}$O	[23]	-59.06	13.4×10^{-3}	$14.8 \pm 1.6 \times10^{-3}$	5.5	$6.8 \pm 0.4 \times10^{-3}$
$1s\,^{18}$O	[22]	-215.76	-18.87	-19.9 ± 0.1	7.40	6.33 ± 0.43
$2p\,^{40}$Ca	[24,25]	-374.60	1.86	1.86 ± 0.08[a]	1.62	1.62 ± 0.11
$2p\,^{44}$Ca	[27]	-374.78	1.92	1.58 ± 0.02	1.84	1.60± 0.07
$3d\,^{108}$Ag	[25]	-922.07	2.27	1.97 ± 0.03	1.24	1.41± 0.05
$4f\,^{208}$Pb	[27]	-1582.19	2.28	1.67 ± 0.02	1.1	1.17± 0.05
$4f\,^{209}$Bi	[28]	-1622.21	2.53	1.83 ± 0.06	1.31	1.24± 0.14

[a]Average experimental values.

A. Shallow states

While our ultimate interest is deeply bound $1s$ and $2p$ levels in heavy nuclei, we need first test and tune our potential by examining shallow pionic atom states. Accordingly, we adjusted the annihilation strengths B_0 and C_0 by fitting the $1s$ and $2p$ levels in pionic ^{16}O [22,23] and the $2p$ level in ^{40}Ca [24,25]. This procedure avoids anomalies associated with the $3d$ levels [26], and determines

$$B_0 = (-0.074 + 0.067i)m_\pi^{-4},$$
$$C_0 = (0.051 + 0.069i)m_\pi^{-6}. \tag{21}$$

We do not expect a potential with as few parameters as ours to give the same level of agreement as a phenomenological one with various strength and size parameters determined in a global search. In Table IV and Fig. 1 we show a comparison between the strong interaction shifts predicted by our potential (the +'s) and various pionic atom data [22–25,27,28]. We see very good agreement for the heavier nuclei, good agreement for the lighter nuclei, and an incongruently large deviation for ^{18}O (recall, we fit B_0 and C_0 to ^{16}O and ^{40}Ca). In general, our level of agreement is comparable to the finite range, momentum space calculations of Cieplý *et al.* [20] — even though the potentials and calculational frameworks differ. For example, Cieplý *et al.* find $B_0 = (-0.093 + i0.042)m_\pi^{-4}, C_0 = (-0.125 + 0.090i)m_\pi^{-6}$, the differences with (21) probably reflecting the differences in $U^{(1)}$ and in the data fit.

B. Deep states

In Table V and Fig. 2 we show the predicted energies and widths of the deeply bound $\pi^-\,^{208}$Pb states. The $E_{\rm EM}$ results are for the pure electromagnetic interactions (Coulomb + vacuum polarization [29]), the $E_{\rm lpott}$ ones for the combined EM plus optical potentials, and the $r1$, $r2$, and $r3$ ones for the r-space calculations of Toki *et al.* [5], Nieves *et al.* [30], and of Konijn *et al.* [31]. Even though our optical potential differs significantly from these others, we see that our calculated binding energies are only slightly larger ($\sim 7\%$) — probably not large enough to change the chance of success of any experimental searches. Our widths, however, are significantly larger and may well change the chance of success of an experimental search.

The differences among the models' predictions increase with binding. Consequently, the origin of the differences may lie in the energy dependencies of the potentials, the wave equations used, or the extrapolations in the complex energy plane. Since the differences are much greater for Γ than Re E, the models for the annihilation potential must also be important (we use a finite range model, the others do not). This is a much greater optical model dependence than $(0.4, 15)\%$ in (Re E, Γ) found by Nieves *et al.*

To further understand the physics of the nonlocal optical potential and test the momentum space calculation,

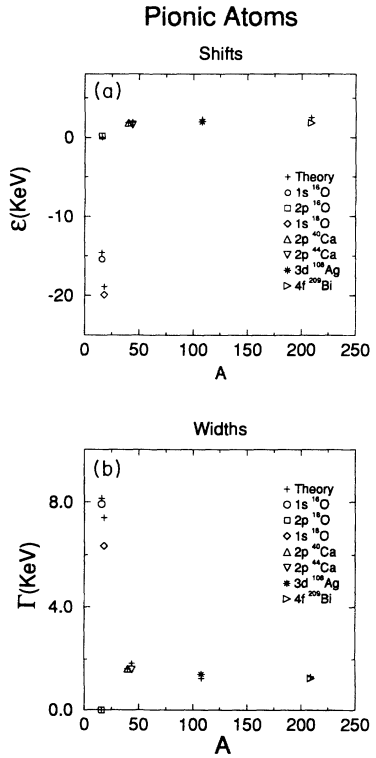

FIG. 1. Comparison of optical potential predictions and measurements of shifts (top) and widths (bottom) for the indicated shallow levels of pionic atoms. Data are from Refs. [22–28].

TABLE V. Theoretical energies and widths in keV for $\pi^- - {}^{208}$Pb. The subscripts $r1$, $r2$, and $r3$ denote r-space calculations of Toki *et al.* [5], Nieves *et al.* [30], and Konijn *et al.* [31].

nl	$E_{\rm EM}$	$E_{\rm lpott}$	E_{r1}	E_{r2}	E_{r3}	$\Gamma_{\rm lpott}$	Γ_{r1}	Γ_{r2}	Γ_{r3}
$1s$	-12302	-7240	-6959	-6778	-6924	754	632	409	63
$2s$	-4492	-3043	-2962	-2902	-2954	208	183	140	13
$2p$	-5957	-5399	-5162	-5105	-5138	619	410	275	154
$3s$	-2262	-1682	-1642	-1613	-1633	88	78	65	5
$3p$	-2707	-2488	-2418	-2395	-2408	201	151	99	52
$3d$	-2831	-2916	-2854	-2858		125	91	56	
$4s$	-1352	-1067	-1045	-1026		45	40	35	
$4p$	-1538	-1436	-1408	-1394	-1394	90	71	46	24
$4d$	-1594	-1639	-1606	-1606		73	52	31	
$4f$	-1579	-1582	-1575	-1582		1.1	1.0	1.0	

we have also constructed the r-space wave functions of the deeply bound states via (17)–(20). In the top of Fig. 3 we display the modulus of the momentum space wave function for the $1s$ state in Pb, and in the bottom of the figure we display the corresponding $\psi_l(r)$. In the comparison to the pure Coulomb wave function, we see that the optical potential introduces structures into $\psi(k)$ similar to those in the potential, and that the strong interaction repels $\psi(r)$ from the nuclear interior. Even though this is a $1s$ state, we also note a node in Re $\psi(r)$ — a consequence of the normalization condition (18) and (19) for complex wave functions. These wave functions are similar in both shape and magnitude to those of Toki *et al.* [5], and should yield similar predictions when used in a DWIA calculation of the formation rate of the state.

In Fig. 4 we plot the probability density [32] $|u_l(r)|^2 \equiv |r\psi_l(r)|^2$ for $1s$, $2s$, and $2p$ states in Pb when there is only the EM potential (dashed curves) and when there is the EM plus nuclear potentials (solid curves). Although the wave function is repelled out of the nucleus for these three states, it is attracted for $3d$ and higher states [5]. This variation in attraction with levels, and the fact that the p states are attracted inwards in lighter nuclei, confirm earlier findings with local coordinate space potentials [33].

C. Nuclear bound states

We have found that the pion-nucleus optical potential is attractive enough to produce broad pion-nucleus resonances, but not attractive enough to actually bind the pion within the interior of the nucleus. Yet we uncovered some interesting features of the pion-nucleus optical potential by progressively increasing its strength and watching the hybrid Coulomb-nuclear state slowly move closer to the nucleus until it becomes a nuclear state at

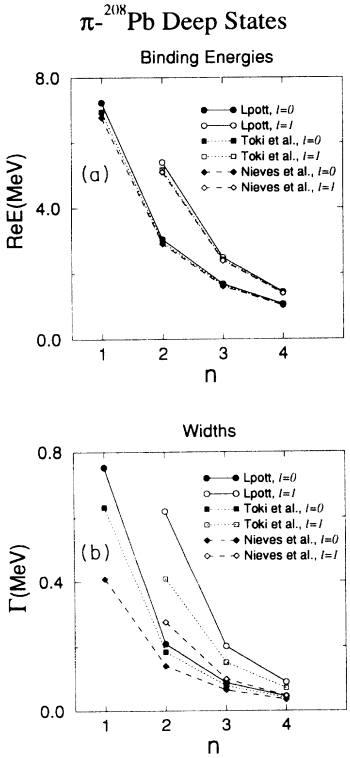

FIG. 2. Energy levels (top) and widths (bottom) of various deeply bound $\pi^-{}^{208}$Pb states. The solid curves derive from the present p-space potential, the others from the r-space potentials of Toki *et al.* [5] and Nieves *et al.* [30].

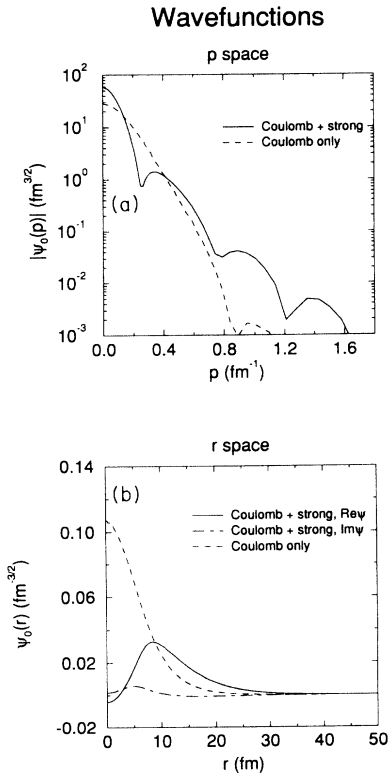

FIG. 3. Momentum-space wave function $\psi_l(p)$ and coordinate-space wave functions $\psi_l(r)$ for π^-Pb $1s$ state. Dashed curves derive from the EM potential alone, solid curves also contain the optical potential, and the dot-dashed curve shows Im $\psi_l(r)$ for the total potential. A logarithmic scale is used for $\psi_l(p)$ to show details of nuclear effect. In the lower part of the figure, the exclusion of the wave function from the nucleus of radius $\sim$ 7.1 fm is evident, as is the node introduced into the wave function.

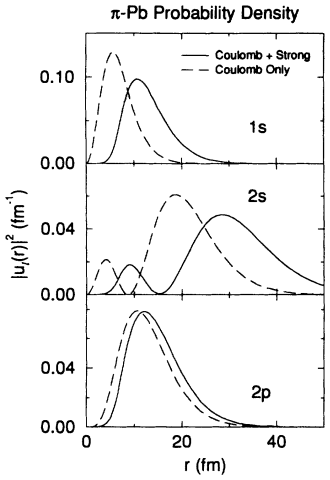

FIG. 4. Probablity density $|u_l(r)|^2 \equiv |r\psi_l(r)|^2$ for the $1s$, $2s$, and $2p$ π^-Pb states. Dashed curves contain only the EM potential, and solid curves EM plus optical potentials. The exclusion of the wave function from the nucleus of radius ~ 7.1 fm is evident, although the node in the real part of the wave function at ~ 2.5, evident in Fig. 3, is not.

about 8–15 fold normal strength.

The existence of nuclear state with increased potential strength is expected for p states in Ca where the level shifts in Table IV are attractive, but may be a surprise for s states where the level shift is repulsive (increasing the strength of a potential does not usually change its effect from repulsion to attraction). To unravel the physics of the normal strength optical potential, we used the radial wave function $u_l(r) \equiv r\psi_l(r)$ to deduce an equivalent local potential which produces this same $u_l(r)$ when used in a nonrelativistic Schrödinger equation:

$$V_{\rm equiv}(r) = \frac{\hbar^2}{u_l(r)2\mu}\left[\frac{d^2u_l(r)}{dr^2} + \left(\frac{2\mu E}{\hbar^2} - \frac{l(l+1)}{r^2}\right)u_l(r)\right]. \quad (22)$$

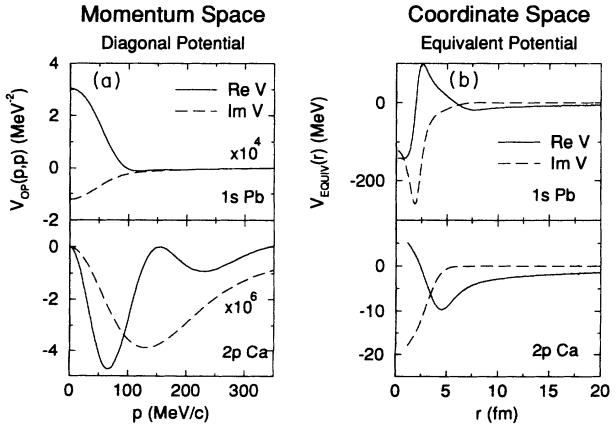

FIG. 5. The diagonal momentum space potentials $V(p,p)$ (left) and equivalent local coordinate space potentials $V_{\rm equiv}(r)$ (right) for the $1s$ state in ^{208}Pb (top) and the $2p$ state in ^{40}Ca (bottom).

The procedure (22) results in the potentials shown in the right-hand side of Fig. 5. Although this procedure has pitfalls near the nodes of $u_l(r)$, the deduced potentials are seen to be realistic enough to always have their imaginary parts absorptive. We see in the lower right-hand corner that $\mathrm{Re}V_{\rm equiv}(r)$ for the normal $2p$ state in Ca has a long-range attraction and a short-range repulsion. As the potential strength is increased, this potential acquires an oscillation in the surface — much like the one expected from the $\nabla \cdot \rho(r)\nabla$ term in the Ericson-Ericson potential (1). In the upper right-hand corner of Fig. 5, we see that $\mathrm{Re}V_{\rm equiv}(r)$ for the normal $1s$ state in Pb has a central attraction in addition to a middle-range repulsion. As these potentials are made stronger, the nuclear state gets formed in the inner attractive regions.

IV. CONCLUSIONS

Our calculations confirm the existence of deep, hybrid Coulomb-nuclear $1s$, $2s$, and $2p$ bound states. However, we find their widths to be significantly greater (20–300 %) than reported previously for quite different potentials [2,5,8], and their binding energies to be slightly ($\sim$ 7%) greater. Although the states remain nonoverlapping, our larger widths may affect experimental searches. Because the differences among models increases with binding, the model dependence appears to arise from our inclusion of energy dependencies in the optical potential, complex energy extrapolations, and our treatment of the finite-range annihilation term, the latter affecting the widths in particular. Our wave functions are similar enough to those of Toki *et al.* [5] so as not to yield major changes in atomic formation rates.

The major uncertainty in this work is the effect of pion annihilation on the optical potential. At present, theory does not appear capable of predicting these higher order terms to the precision needed for comparisons with pionic atom level, and so the potential strengths are adjusted phenomenologically.

We have also looked for nuclear bound states of pions internal to the nucleus. We found only resonances and had to increase the strength of the potential at least eightfold before bound states appeared. In the process, we discovered that at normal strength the real part of the effective local potential for a $1s$ pion in Pb has an inner attraction in addition to a strong, outer repulsive barrier. Likewise, a $2p$ pion in Ca is found to have an inner repulsion in addition to an outer attraction. It is these attractive parts which bind the pion within the nucleus as the potential strength is increased.

From a computational viewpoint, we have shown that pionic atom energies can be calculated accurately in momentum space with a microscopic, nonlocal, and energy-dependent optical potential. We have done it by searching for the poles of the T matrix for the combined Coulomb plus nuclear potential, in contrast to more usual eigenfunction methods [13,20].

ACKNOWLEDGMENTS

It is our pleasure to thank Eli Friedman for the conversations and assurances which stimulated the present

study. We also wish to thank Iraj Afnan, Bill Kaufman, Anne Trudel, D. Frekers, Al Stetz, Carmen Garcia-Recio, and Avraham Gal for illuminating discussions. We gratefully acknowledge support from the U.S. Department of Energy under Grant No. DE-FG06-86ER40283 and the people at the National Institute for Nuclear Theory, Seattle for their hospitality during part of this work.

APPENDIX A: RELATIVISTIC EFFECTS AND NUMERICAL PRECISION

The spin-zero pion is usually described by the Klein-Gordon equation (KGE):

$$\left[E - V^{\rm Coul}\right]^2 \psi(r) = \left[-\nabla^2 + (\mu + V^{\rm opt})^2\right] \psi(r)$$
$$\simeq \left[-\nabla^2 + \mu^2 + 2\mu V^{\rm opt}\right] \psi(r), \quad \text{(A1)}$$

where the approximate form on the extreme right is usually used [2,5,30] to avoid technical difficulties (Kwon and Tabakin [13] have indicated how the quadratic term can be handled in momentum space). As given in Eq. (13), we solve the relativistic Schrödinger equation (RSE). In this appendix, we indicate how predictions of these two equations differ from each other and how much our numerical solutions differ from analytic ones for point-particle deep states.

The Bohr energies are the well-known solutions of the SE for a point Coulomb potential. For the KGE, the analytic solution has the expansion [34,35]:

$$E_{nl}^{\rm KGE} \simeq mc^2 - \frac{mc^2(Z\alpha)^2}{2n^2} - \frac{mc^2(Z\alpha)^4}{2n^4}\left(\frac{n}{l+\frac{1}{2}} - \frac{3}{4}\right) + O(\alpha^6). \quad \text{(A2)}$$

To compare the KGE with the two-particle SE, we use a reduced mass μ in the second term of (A2), and the pion mass m_π in the first term.

Columns 2 and 3 in Table II indicate our numerical precision by comparing the computed and analytic results for the SE (we know of no analytic results for the RSE). We see that the numerical results are good out to the fifth decimal place, and that the computed $2s$ and $2p$ levels are degenerate (as well they should be) within numerical precision—even though the partial-wave potentials are quite different. Columns 3 and 4 in Table II and columns 2 and 3 in Table III indicate that relativistic effects are significant: 2% for ^{40}Ca-1s, 70% for ^{208}Pb-1s, and 48% for ^{208}Pb-2s. In contrast, columns 5 and 6 in Table II and columns 3 and 4 in Table III indicate that both the RSE and the KGE using the reduced mass remove the degeneracy with l and include similar enough relativistic corrections for the differences to lie in the fourth significant figure. (The effect would be bigger for s states in Pb, but the KGE point-Coulomb solution is pathological for $l = 0$ and $Z\alpha > \frac{1}{2}$.)

[1] R. Seki, Phys. Rev. C **5**, 1196 (1972); J.H. Koch, M.M. Sternheim, and J.F. Walker, *ibid.* **5**, 381 (1972); T.E.O. Ericson and F. Schneck, Nucl. Phys. **B19**, 450 (1970).
[2] E. Friedman and G. Scoff, J. Phys. G **11** (1985).
[3] S. Hirenzaki, T. Kajino, K.-I. Kubo, H. Toki, and I. Tanihata, Phys. Lett. B **194**, 20 (1987).
[4] H. Toki and T. Yamazaki, Phys. Lett. B **213**, 129 (1988).
[5] H. Toki, S. Hirenzaki, T. Yamzaki, and R.S. Hayano, Nucl. Phys. **A501**, 653 (1989).
[6] M. Iwasaki, A Trudel, A. Celler, O. Käusser, T.S. Hayano, R. Helmer, R. Henderson, S. Hirenzaki, K.P. Jackson, Y. Kuno, N. Matsuoka, J. Mildenberger, C.A. Miller, H. Outa, H. Sakai, H. Toki, M. Vetterli, Y. Watanabe, T. Yamazaki, and S. Yen, Phys. Rev. C **43**, 1099 (1991).
[7] H. Toki, S. Hirenzaki and T. Yamazaki, Nucl. Phys. **A530**, 679 (1991).
[8] J. Nieves and E. Oset, Phys. Lett. B **282**, 24 (1992).
[9] W.B. Kaufmann, P.B. Siegel, and W.R. Gibbs, Arizona State University report, 1992.
[10] R.H. Landau, S.C. Phatak, and F. Tabakin, Ann. Phys. **78**, 299 (1973); R.H. Landau, Comput. Phys. Commun. **28**, 109 (1982).
[11] R.H. Landau and F. Tabakin, Nucl. Phys. **A231**, 445 (1974).
[12] A. W. Thomas and R. H. Landau, Phys. Rep. **58**, No. 3, 121 (1980); R.H. Landau and A. W. Thomas, Nucl. Phys. **A302**, 461 (1978).
[13] Y.R. Kwon and F. Tabakin, Phys. Rev. C **18**, 932 (1978); D.P. Heddle, Y.R. Kwon, and F. Tabakin, Comput. Phys. Commun. **38**, 71 (1985).
[14] J. Blomqvist, Nucl. Phys. **B48** 95 (1972).
[15] E. Friedman, personal communication.
[16] H. De Vries, C. W. De Jager, and C. De Vries, At. Data Nucl. Data Tables **36**, 495 (1987).
[17] G. Kalbermann, E. Friedman, A Gal, and C.J. Batty, Nucl. Phys. **A503**, 632 (1989); C.J. Batty, E. Friedman, A Gal, and G. Kalbermann, *ibid.* **A535**, 548 (1991).
[18] L.L. Foldy and R.A. Krajcik, Phys. Rev. Lett. **32**, 1025 (1974); F. Coester, Helv. Phys. Acta. **38**, 7 (1965).
[19] R.H. Landau, Phys. Rev. C **27**, 2191 (1983).
[20] A. Cieplý, M. Gmitro, R. Mach, and S.S. Kamalov, Phys. Rev. C **44**, 713 (1991); M. Gmitro, S.S. Kamalov, and R. Mach, *ibid.* **36**, 1105 (1987).
[21] E. Hernàndez and A. Mondragon, Phys. Rev. C **29**, 722 (1984).
[22] I. Schwanner, R. Abela, G. Backenstoss, W. Kowald, P. Pavlopoulos, L. Tauscher, H.J. Weyer, P. Blüm, M. Dörr, W. Fetscher, D. Gotta, R. Guigas, H. Koch, H. Poth, G. Schmidt, and H. Ullrich, Phys. Lett. **96B**, 268 (1980).
[23] G. De Chambrier, W. Beer, F.W.N. De Boer, K. Bos, A.I. Egorov, M. Eckhause, K.L. Giovanetti, P.F.A. Goudsmit, B. Jeckelmann, K.E. Kir'yanov, L.N. Kodurova, L. Lapina, H.J. Leisi, V.I. Marushenko, A.F. Mezentsev, A.A. Petrunin, A.G. Sergeev, A.I. Smirnov, G. Strassner, V.M. Suvorov, A. Vacchi, and D. Wieser, Nucl. Phys. **A442**, 637 (1985).
[24] R.J. Powers, K.C. Wang, M.V. Hoehn, E.B. Shera, H.D. Wohlfahrt, and A.R. Kunselman, Nucl. Phys. **A336**, 475 (1980).

[25] C.J. Batty, S.F. Biagi, E. Friedman, S.D. Hoath, J.D. Davies. G.J. Pyle, G.T.A. Squier, D.M. Asbury, and H. Guberman, Nucl. Phys. **A322**, 445 (1979).

[26] R. Seki, K. Masutani, M. Oka, and K. Yazaki, Phys. Lett. **97B,** 200 (1980); R. Seki and K. Masutani, Phys. Rev. C **27**, 2799 (1983); R. Seki, K. Masutani, and K. Yazaki, *ibid.* **27**, 2817 (1983).

[27] C.J. Batty, S.F. Biagi, E. Friedman, S.D. Hoath, J.D. Davies, G.J. Pyle, G.T.A. Squire, D.M. Asbury, and M. Leon, Phys. Lett. **81B**, 165 (1979).

[28] E. Friedman, H.J. Gils, H. Rebel, and Z. Majka, Phys. Rev. Lett. **41**, 1220 (1978).

[29] The vacuum polarization increases the binding by 0.5% and the width by 2%, which may be significant, but not compared to the model dependence.

[30] J. Nieves, E. Oset, and C. Garcia-Recio, Nucl. Phys. **A554**, 509 (1993).

[31] J. Konijn, C.T.A.M. de Laat, A. Taal, and J.H. Koch, Nucl. Phys. **A519**, 773 (1990).

[32] Because we use the Gamow state normalization (18) and (19), it can be argued that the proper probability density is $[\mathrm{Re}\ \psi_l(k)]^2 - [\mathrm{Im}\ \psi_l(k)]^2$. The difference is not significant for the present case.

[33] M. Ericson, T.E.O. Ericson, and M. Krell, Phys. Rev. Lett. **22**, 1189 (1969).

[34] R.H. Landau, *Quantum Mechanics II* (Wiley, New York, 1990).

[35] H.A. Bethe and R. Jackiw, *Intermediate Quantum Mechanics* (Benjamin, Reading, 1968).